Cathodic corrosion

Hersbach, T.J.P.

6

Enhancement of Oxygen Reduction Activity of Pt(111) through Mild Cathodic Corrosion

*The oxygen reduction reaction (ORR) is a crucial half-reaction of fuel cells. Effectively promoting the ORR is therefore of prime importance in developing commercially viable fuel cells. Unfortunately, many common ORR catalysts have activities that are well below the theoretically predicted optimum. This is due to many catalysts binding reaction intermediates like adsorbed hydroxide (*OH) too strongly. In the current chapter, we explore a new approach to optimizing *OH binding on existing catalysts: catalyst pretreatment with cathodic corrosion. We do this by mildly cathodically corroding a Pt(111) single crystal, in an effort to create catalytic sites with optimized *OH binding strength. Electrochemical characterization of the corroded Pt(111) electrode reveals the creation of step sites on the surface. These sites appear more active towards the ORR than 'normal' stepped sites. They are therefore likely concave sites with optimized *OH binding properties. This result presents cathodic corrosion as a method to optimize existing catalysts for the ORR and other structure-sensitive reactions.*

6.1 Introduction

Anthropogenic climate change has stimulated large-scale efforts to shift from fossil to renewable sources of energy.[1,2] A prominent approach for achieving this shift is the 'hydrogen economy', in which renewable energy is used to generate hydrogen from water.[3,4] This hydrogen could be stored, transported and later oxidized in fuel cells to generate electricity where it is needed. Unfortunately, the performance of fuel cells is currently severely limited by the counter reaction of hydrogen oxidation: the oxygen reduction

This chapter will form the basis of a manuscript that will be submitted to a peer-reviewed scientific journal.

reaction (ORR).[5] Catalyzing this reaction with high current densities and at low overpotentials is therefore an important focus area in electrochemistry.

The most active metallic ORR catalysts are platinum group metals.[6] However, even these active catalysts are typically limited in their performance, because they bind reaction intermediates like adsorbed oxygen (*O) and adsorbed hydroxide (*OH) too strongly.[5] For example, theoretical calculations indicate the binding of *OH on the (111) facet of platinum to be too strong by approximately $0.1\ eV$.[7] This would suggest that the activity of platinum-group metals can be enhanced by weakening the *OH binding strength.[8]

The *OH binding strength can be weakened by creating alloy catalysts:[9] model alloys, like Pt_3Ni(111) and PtCo(111), show strongly improved activity with regard to Pt(111).[10–12] However, translating these model catalysts into their industrially relevant nanoparticle equivalents is not straightforward, with many alloy nanoparticles being unstable and changing their composition under ORR conditions.[4,7,13,14] It might therefore be more prudent to generate active ORR catalysts from single elements like platinum.

This approach would rely on tuning the catalyst's surface structure, since the platinum ORR activity is sensitive to the exposed surface sites: in $HClO_4$, the three Pt basal planes increase in activity in the order (100) < (111) < (110).[15] Even more active are stepped surfaces.[16–18] Though steps contain strongly *OH-binding sites at the top of the step, they also contain concave sites at the bottom of the step which bind *OH weaker than Pt(111).[19] Notably though, most of these concave sites bind *OH slightly too weakly and thus overshoot the activity optimum for the ORR.[20] Instead, optimal activity can be achieved by removing atoms from flat platinum surfaces to create sites that bind *OH nearly optimally.[20]

Atom removal to optimize *OH binding may be achieved by cathodic corrosion, since Chapter 2 and 4 identified the creation of etch pits during cathodic corrosion. Though these roughly 30 nm-wide pits are larger than the optimal 1 nm-wide pits,[20] the aforementioned chapters also indicate the presence of smaller etching features that are undetectable in scanning electron microscopy. In an effort to generate these smaller sites with optimal ORR reactivity, the current chapter focuses on modifying Pt(111) through mild cathodic corrosion in 1 M NaOH. As will be demonstrated, this approach indeed enhances the ORR activity of Pt(111); this enhancement is likely caused by creating sites with more optimal *OH binding. These results present cathodic corrosion as a viable method to enhance the activity of monometallic platinum electrocatalysts. As such, the present work opens up strategies for modifying commercial catalysts to generate optimum binding

sites with superior catalytic activity.[19]

6.2 Materials and methods

6.2.1 Cleaning and sample preparation

All water used in this work (resistivity $> 18.2\ M\Omega \cdot cm$, TOC $< 5\ ppb$) was purified with a Millipore MilliQ system. All glassware was cleaned from organic contamination by soaking overnight in an aqueous solution of $1\ g \cdot L^{-1}$ $KMnO_4$ (Fluka, ACS reagent) and $0.5\ M$ H_2SO_4 (Fluka, ACS reagent). Before experiments, this solution was drained and residual MnO_4^- was decomposed by immersing the glassware in dilute H_2O_2 (Merck, Emprove exp). This solution was subsequently drained and all glassware was boiled in water six times to remove inorganic contaminations, including (bi)sulfate from the cleaning solution.

After cleaning, two three-electrode glass cells were prepared: one cell for sample characterization and one cell for ORR catalysis. These cells were filled with $0.1\ M$ $HClO_4$ (Fluka, TraceSelect) and each contained a Pt counter electrode (Mateck, 99.9%) and an internal reversible hydrogen electrode (RHE) which used a constant hydrogen (Linde, 6.0 purity) flow. The RHE was connected to an auxiliary Pt electrode in the main cell compartment with a $4\ \mu F$ capacitor, in order to reduce high-frequency noise during electrochemical experiments.[21]

In addition to these two glass cells, a third single-compartment cell made of fluorinated ethylene propylene (FEP) was used for cathodic corrosion. This cell was filled with $1\ M$ NaOH (Merck, Suprapur), contained a commercial 'Hydroflex' RHE (Gaskatel) and a dimensionally stable anode counter electrode, provided by Magneto Special Anodes. This staff-shaped anode consisted of titanium, coated with a porous iridium mixed metal oxide. Before use, this electrode was cleaned by rinsing it with H_2O_2, since it could not be cleaned by flame-annealing or soaking in the $KMnO_4$ cleaning solution; annealing would destroy the electrode, whereas soaking led to $KMnO_4$ being absorbed into the oxide. This $KMnO_4$ could not be removed by boiling the electrode and would therefore be expelled into the working solution when experiments induced oxygen evolution on the counter electrode. Fortunately, the H_2O_2 rinsing procedure proved adequate in cleaning the electrode, since no onset shifts like those observed in Chapter 4 were observed.

Prior to each experiment, working electrodes were prepared by flame-annealing them with a propane torch for approximately 20 seconds. The electrodes were then cooled down in a glass cooler in a reducing H_2/Ar (Linde, 6.0 purity) atmosphere. After cooling,

the electrodes were protected with a droplet of deoxygenated water from the cooling flask and transferred to one of the electrochemical cells. The electrodes used in this study were a home-made 2.3 mm diameter bead-type polycrystalline Pt electrode (Pt(poly)); a 2.1 mm diameter bead-type Pt(100) electrode (iCryst); a 2.5 mm diameter bead-type Pt(110) electrode (iCryst); and a 3 mm diameter, 2 mm high cylindrical Pt(111) crystal (Surface Preparation Laboratory). Cyclic voltammograms for these electrodes are shown in Fig. C.1.

6.2.2 Electrochemistry

Electrochemical experiments were performed with a Bio-Logic VSP-300 potentiostat. After setting up the glassware, cyclic voltammograms were run in both glass cells to ensure the cleanliness of the working solutions. Specifically, each cell was deaerated by purging the electrolyte with argon (Linde, 6.0 purity) for at least 30 minutes. Then, 4 cyclic voltammograms (CVs) of the Pt(111) electrode were recorded in hanging meniscus configuration at a scan rate of 50 $mV \cdot s^{-1}$, between 0.06 and 0.9 V *vs.* RHE, while maintaining deaeration by flowing argon over the working electrolyte. Special attention was paid to the presence of (bi)sulfate, which significantly affects the oxygen reduction activity.[16,17] (Bi)sulfate can easily be detected in Pt(111) voltammograms, since it causes a distinct reductive feature between 0.45 and 0.55 V *vs.* RHE at concentrations as low as 10^{-6} M.[22] If no signs of (bi)sulfate were present and the voltammograms did not change shape between cycles, the cells were considered to be clean. After establishing cleanliness, the argon flow in the catalysis cell was replaced by O_2 (Linde, 6.0 purity), which was bubbled through the working electrolyte for at least 10 minutes to ensure oxygen saturation.

Each experiment started by running 4 Pt(111) CVs in the characterization cell as described above, to validate the cleanliness and ordering of the surface. The Pt(111) electrode was then rinsed and immersed for at least 1 mm in the corrosion cell. In this cell, the cell resistance was determined through impedance spectroscopy at 0.5 V *vs.* RHE, at a 100 kHz frequency and a 20 mV sine wave amplitude.[23] This resistance value was used to subsequently apply a 85% IR-corrected potential to the electrode for 60 seconds, in order to modify the electrode through cathodic corrosion. Following modification, the electrode was removed under potential control, rinsed and moved to the characterization cell. In this cell, the state of the electrode surface was characterized by running 4 cyclic voltammograms between 0.06 and 0.7 V *vs.* RHE. The 0.7 V potential bound was chosen as a safe upper limit where none of the cathodically produced sites would be

removed through oxidation of the surface.

After characterization, the ORR activity of the modified electrode was assessed in the hanging meniscus rotating disk (HMRD) configuration.[24] To this end, the electrode was mounted in a home-made electrode holder that was subsequently screwed into the shaft of a Pine rotator. The electrode was lowered into the catalysis cell, where the oxygen now flowed over the electrolyte solution to maintain oxygen saturation during experiments. In this cell, a meniscus was made between the electrode and the electrolyte while polarizing the electrode at 0.06 V *vs.* RHE. After making contact, the cell resistance was determined through impedance spectroscopy at 0.9 V *vs.* RHE. The electrode potential was then held at 0.06 V *vs.* RHE for 5 seconds before testing the catalytic activity of the electrode with cyclic voltammetry; two CVs were run between 0.06 and 0.9 V *vs.* RHE, at a scan rate of 50 $mV \cdot s^{-1}$. The electrode rotation rate was then automatically changed by the potentiostat to 200 rpm, the current was allowed to stabilize for 5 seconds at 0.06 V *vs.* RHE and two CVs were run between 0.06 and 0.9 V *vs.* RHE. This step was repeated to obtain additional CVs at rotation rates of 400, 900, 1600 and 2500 rpm.

6.3 Results and discussion

In this chapter, we assess the effect of mild cathodic corrosion and the subsequent change in ORR activity for Pt(111) as follows. First, as in previous chapters, blank cyclic voltammograms (CVs) of corroded and uncorroded Pt(111) were recorded. These CVs are presented first. Then, the activity activity of the Pt(111) electrode was studied in the hanging meniscus rotating disk (HMRD) configuration.[24] The proper functioning of the HMRD setup will be discussed briefly, followed by the recorded ORR activity and discussion of the presented results.

6.3.1 Cathodic corrosion of Pt(111)

Blank CVs of Pt(111), before and after cathodic polarization in 1 M NaOH are presented in Fig. 6.1. As can be seen, the uncorroded Pt(111) electrode contains the characteristic hydrogen adsorption and desorption features between 0.06 and 0.4 V *vs.* RHE, followed by the double layer region and subsequent adsorption and desorption of OH between 0.5 and 0.9 V *vs.* RHE.[25] Importantly, no peaks are visible at 0.13 and 0.29 V *vs.* RHE. This indicates that no electrochemically observable peak sites are present on the electrode before cathodic polarization.[26]

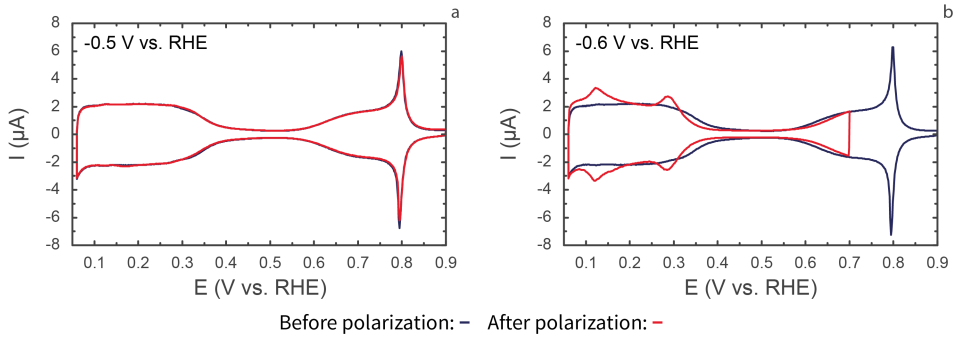

Fig. 6.1 | Cyclic voltammograms of Pt(111) before (blue trace) and after (red trace) cathodic polarization in 1 M NaOH at -0.5 V *vs.* RHE **(a)** and -0.6 V *vs.* RHE **(b)**. Voltammograms were recorded in 0.1 M $HClO_4$, at a scan rate of 50 $mV \cdot s^{-1}$.

Similarly, no additional peaks are present after polarizing Pt(111) at -0.5 V *vs.* RHE in 1 M NaOH. This indicates no change in the electrode structure when polarizing it before the cathodic corrosion onset potential. In contrast, pronounced changes are visible after polarizing the electrode at the onset potential found in Chapter 4: -0.6 V *vs.* RHE. This treatment causes the formation of both (110) steps (0.13 V *vs.* RHE) and (100) steps (0.29 V *vs.* RHE). These changes appear to be largely independent of the corrosion potential, as is illustrated in Fig. C.2 Additionally, the onset of OH adsorption has shifted positively by about 0.02 V, which indicates a slightly weakened *OH adsorption strength on the (111) terrace of the corroded surface.[20] Such weakened binding should promote the ORR activity for the corroded electrode.

6.3.2 HMRD configuration

The ORR activity is assessed in the HMRD configuration.[24] This configuration differs from the conventional rotating disk electrode (RDE) configuration, because the working electrode is not encased in a shaft and submerged into the working solution. Instead, the bead- or cylinder-type crystal is mounted in a modified RDE rotator and contact with the side of the electrode is prevented by elevating the electrode into a hanging meniscus configuration. Though this configuration allows for the convenient use of standard single crystal electrodes, care has to be taken to make sure that the HMRD behaves like a classical RDE electrode.

Specifically, the height of the electrode has to be controlled carefully:[24] if the electrode were too low, wetting of the side would occur and the catalytic activity of sites other

than the desired facet would be probed. This would cause an increased absolute slope in the Levich plot. In contrast, if the electrode were too high, the meniscus would be constrained. This would lead to reduced mass transport and an offset in the ORR Levich plots.

Levich plots were therefore constructed for each electrode to verify the validity of the HMRD setup for the investigated system. A set of ORR voltammograms used for these Levich plots is displayed in Fig. C.3. Additional exemplary Levich plots are displayed for each electrode in Fig. C.4. All reported data were measured on electrodes with zero or near-zero Levich plot offsets and Levich slopes within several percent of the theoretically expected value, based on literature parameters for the solubility and diffusion coefficient of oxygen in $0.1\ M\ HClO_4$.[27] A notable exception to this statement is the employed Pt(110) electrode, which consistently had *lower* Levich slopes. We attribute this to an unexpected decrease in the effective electrode surface area, which is compensated for in the following normalized ORR activity assessment. With the exception of this electrode, all electrodes behaved as expected, such that the HMRD setup can be used to accurately assess the ORR activity of the corroded Pt(111) electrodes.

6.3.3 ORR enhancement by cathodic corrosion

The ORR activity for a corroded Pt(111) electrode, a polycrystalline electrode and the three basal planes of platinum is displayed in Fig. 6.2. In this plot, all currents are normalized by the absolute limiting current density for each electrode. This normalization accounts for minor variations in the limiting current due to small variations in the meniscus height[18] and small deviations in the alignment of the electrode.[12] The normalization therefore allows for objective comparison of the ORR activity in the HMRD configuration.[18]

As can be seen in Fig. 6.2, the ORR activity at $0.9\ V$ *vs.* RHE follows the order Pt(100) < Pt(111) < Pt(110). This activity trend is in good agreement with both experimental results and recent density functional theory calculations.[15,19,20,28] A similar activity is achieved for Pt(poly), which has comparable activity to Pt(111). However, the corroded Pt(111) electrode is more active than any of the other studied crystals. This indicates that cathodic corrosion is indeed able to enhance the ORR activity of a Pt(111) electrode.

The activity enhancement through cathodic corrosion is more readily apparent from the quantitative activity assessment in Fig. 6.3. In Fig. 6.3, the absolute normalized current at $0.9\ V$ is plotted for each electrode. In Panel **b** of this figure, the activity of both Pt(111) and (100) show excellent quantitative agreement with well-prepared electrodes

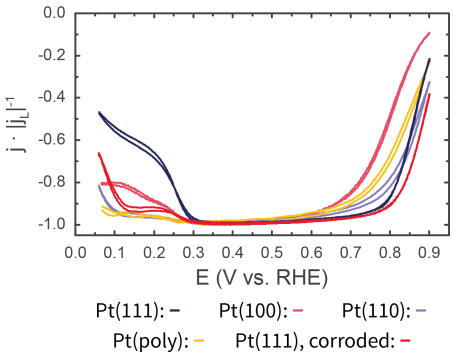

Fig. 6.2 | Cyclic voltammograms for oxygen reduction on Pt(111), Pt(100), Pt(110), Pt(poly) and Pt(111) which was corroded at $-0.6\ V$ *vs.* RHE in 1 M NaOH. The electrode rotation rate was 1600 rpm. Voltammograms were recorded in oxygen-saturated 0.1 M $HClO_4$, at a scan rate of 50 $mV \cdot s^{-1}$.

from the work from Feliu *et al.*[28] A more qualitative agreement is obtained for Pt(poly) and Pt(110), which are respectively more and less active than similar previously studied electrodes.[28,29] The increased Pt(poly) activity can be ascribed to a slightly different state of the surface, which can be expected for different polycrystalline electrodes. Similarly, the reduced activity of Pt(110) is caused by the crystal's high sensitivity to reconstructed 1×2 domains on the surface: if less reconstructed domains are formed during the cooling of the crystal, the ORR activity is reduced as well.[30] This remarkable sensitivity of Pt(110) to variations in the crystal cooling conditions is also responsible for the slightly larger error bar for Pt(110) in Fig. 6.3 **b**. From Panel **b**, it therefore appears that all electrodes are as active as expected from literature.

With all uncorroded single crystals behaving in accordance with previous literature, the activity of cathodically treated Pt(111) can be assessed quantitatively (Fig. 6.3 **a**). In Fig. 6.3 **a**, it can be seen that the activity of Pt(111) is not enhanced if the polarization potential is below the onset potential that was established in Chapter 4. However, the Pt(111) ORR activity at $0.9\ V$ *vs.* RHE increases sharply after cathodic treatment at or below the onset potential of $-0.6\ V$ *vs.* RHE: the normalized activity improves from 0.22 to 0.38. This improvement corresponds to an increase in the kinetic current density (j_k) from 2.8 to 6.6 $mA \cdot cm^{-2}$, as can be seen in Fig. C.5. This enhancement of both j_k and the normalized activity decreases slightly at more negative corrosion potentials, but increases again to 0.37 (6.4 $mA \cdot cm^{-2}$) at $-1.0\ V$ *vs.* RHE. It therefore appears that electrode

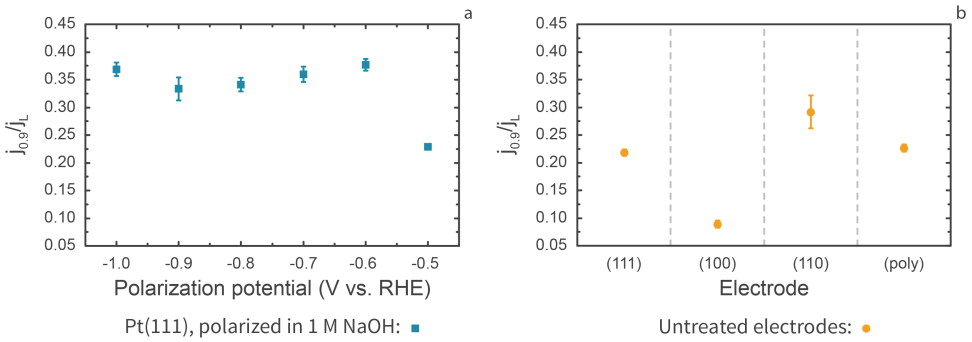

Fig. 6.3 | Normalized ORR activity of corroded Pt(111) (blue squares), as function of the polarization potential **(a)** and of uncorroded electrodes (yellow circles) **(b)**. Rotation rate: 1600 *rpm*. Each data point is the average of 3 or more experiments. Error bars represent one standard deviation.

pretreatment with cathodic corrosion can strongly enhance the oxygen reduction activity of Pt(111).

6.3.4 Discussion

Though the data in Fig. 6.3 and Fig. C.5 indicate that cathodic corrosion can more than double the kinetic ORR current density of Pt(111), it is instructive to rationalize the exact cause of this improvement. Specifically, one might wonder whether the improvement is simply caused by the creation of step sites or by the formation of sites with optimal generalized coordination numbers.

The presence of step sites on Pt(111) is known to enhance the ORR activity.[16–18] If the presence of 'normal' (110) and (100) sites were the cause of the presently reported activity enhancement, the enhancement should therefore correlate roughly to the amount of steps.[18] However, the corroded step sites appear to have much higher activities than most stepped single crystals:[28] only crystals with very high step densities surpass the normalized activity of the corroded electrodes. For example, our most active electrodes are as active as Pt(332), which has one (110) step for every five (111) terrace atoms[31] and a normalized activity of 0.38.[28] By qualitatively comparing the CVs of Pt(332) and other stepped single crystals with those in Fig. 6.1, one can conclude that the stepped crystals possess a much higher step density than the corroded (111) electrodes.[31,32] Each step on a stepped single crystal therefore has a *lower* ORR activity contribution than a step on corroded Pt(111).

This reduced contribution of steps on stepped single crystals is likely due to those

steps binding *OH too weakly and thus overshooting the per-step ORR activity optimum.[20] Since these steps are less active than those created in the current work, it appears that the current steps possess a more optimized *OH binding strength. In fact, the cathodically created steps are approximately as active as optimal binding sites that can be created through anodic cycling.[20] Through such cycling, a 15 % surface area increase through active site formation led to a current densities of approximately $7.4\ mA \cdot cm^{-2}$. Such area increases and current densities are comparable to those presented here. It is therefore highly likely that both the previously reported anodically created sites[20] and the cathodically created sites presented here have similar concave geometries with optimized *OH binding.

A final argument for this conclusion is that optimized concave pits are rather small,[20] being approximately 3 atoms ($\sim 0.9\ nm$)[33] wide and having the optimally coordinated atom at the bottom of the pit. Such sites should only be present after mild cathodic corrosion, where no etch pits are detectable in SEM yet. Accordingly, more pronounced corrosion will create overlapping etch pits, which contain less optimally coordinated Pt atoms per square nanometer. Such strongly corroded electrodes should then have a lower ORR activity than those in Fig. 6.3. This is demonstrated in Fig. C.6, which displays exploratory experiments of Pt(111), corroded in 10 M NaOH. As the figure shows, corrosion at $-0.4\ V$ *vs.* RHE creates a surface that is similar to those created in 1 M NaOH. This surface also has a comparable normalized activity of 0.32. However, a monotonic activity decrease is observed for more pronounced cathodic corrosion at $-0.5\ V$ *vs.* RHE and below. This indicates that the creation of more step sites through cathodic corrosion does not necessarily correlate to an enhanced activity, since Chapter 2 and 4 indicate this corrosion to create large sites overlapping sites that are not beneficial to the overall ORR activity.

Based on the aforementioned considerations, it appears that cathodic corrosion is a suitable technique for creating active ORR sites. This opens possibilities for creating active sites on nanocatalysts such as (111)-oriented nano-octahedra that could benefit from the presence of additional concave sites.[14,19] Though modifying nanocatalysts will require overcoming challenges like ensuring nanoparticle adhesion during cathodic corrosion, such modification might be a viable strategy for producing industrially relevant ORR catalysts. This reasoning is supported by encouraging recent results, where cathodic corrosion in methanol was shown to improve the distribution of various types of metallic nanoparticles.[34]

Cathodic corrosion as a catalyst enhancement strategy is not limited to oxygen reduction on platinum. The current approach can easily be extended to structure-sensitive reactions like glycerol oxidation and ammonia oxidation,[35,36] or to different metal catalysts. These applications of cathodic corrosion can further be directed by the guidelines in Chapter 4.

6.4 Conclusions

Summarizing, the current chapter has demonstrated that the oxygen reduction activity can be significantly enhanced by cathodic corrosion. This enhancement is likely not caused by the creation of 'normal' step sites, but instead by the formation of active concave sites on the Pt(111) surface.[20] These results strongly support the notion that cathodic corrosion can be used to pre-treatreat metallic nanoparticles to improve catalytic activity and selectivity. As such, cathodic corrosion may play a vital role in future electrocatalyst improvement.

6.5 Acknowledgements

The authors thank Magneto Special Anodes for providing dimensionally stable anode counter electrodes.

References

1. Anderson, K. & Peters, G. The trouble with negative emissions. *Science* **354** (2016).
2. Oreskes, N. in *Climate Modelling* (eds Lloyd, E. A. & Winsberg, E.) 31–64 (Palgrave Macmillan, Cham, 2018).
3. Bockris, J. O. A Hydrogen Economy. *Science* **176,** 1323–1323 (1972).
4. Katsounaros, I. & Koper, M. T. M. in *Electrochemical Science for a Sustainable Society* 23–50 (Springer International Publishing, Cham, 2017).
5. Nørskov, J. K. *et al.* Origin of the overpotential for oxygen reduction at a fuel-cell cathode. *Journal of Physical Chemistry B* **108,** 17886–17892 (2004).
6. Markovic, N. Surface science studies of model fuel cell electrocatalysts. *Surface Science Reports* **45,** 117–229 (2002).
7. Stephens, I. E. L., Bondarenko, A. S., Grønbjerg, U., Rossmeisl, J. & Chorkendorff, I. Understanding the electrocatalysis of oxygen reduction on platinum and its alloys. *Energy & Environmental Science* **5,** 6744 (2012).
8. Kulkarni, A., Siahrostami, S., Patel, A. & Nørskov, J. K. Understanding Catalytic Activity Trends in the Oxygen Reduction Reaction. *Chemical Reviews* **118,** 2302–2312 (2018).
9. Greeley, J. *et al.* Alloys of platinum and early transition metals as oxygen reduction electrocatalysts. *Nature Chemistry* **1,** 552–556 (2009).

10. Stamenkovic, V. R. *et al.* Improved Oxygen Reduction Activity on Pt3Ni(111) via Increased Surface Site Availability. *Science* **315,** 493–497 (2007).
11. Stamenkovic, V. R. *et al.* Trends in electrocatalysis on extended and nanoscale Pt-bimetallic alloy surfaces. *Nature Materials* **6,** 241–247 (2007).
12. Wakisaka, M. *et al.* Unprecedented dependence of the oxygen reduction activity on Co content at Pt Skin/Pt-Co(111) single crystal electrodes. *Electrochemistry Communications* **67,** 47–50 (2016).
13. Greeley, J. & Nørskov, J. K. Combinatorial Density Functional Theory-Based Screening of Surface Alloys for the Oxygen Reduction Reaction. *The Journal of Physical Chemistry C* **113,** 4932–4939 (2009).
14. Strasser, P., Gliech, M., Kuehl, S. & Moeller, T. Electrochemical processes on solid shaped nanoparticles with defined facets. *Chemical Society Reviews* **47,** 715–735 (2018).
15. Marković, N., Adžić, R., Cahan, B. & Yeager, E. Structural effects in electrocatalysis: oxygen reduction on platinum low index single-crystal surfaces in perchloric acid solutions. *Journal of Electroanalytical Chemistry* **377,** 249–259 (1994).
16. Maciá, M. D., Campiña, J. M., Herrero, E. & Feliu, J. M. On the kinetics of oxygen reduction on platinum stepped surfaces in acidic media. *Journal of Electroanalytical Chemistry* **564,** 141–150 (2004).
17. Kuzume, A., Herrero, E. & Feliu, J. M. Oxygen reduction on stepped platinum surfaces in acidic media. *Journal of Electroanalytical Chemistry* **599,** 333–343 (2007).
18. Gómez-Marín, A. M. & Feliu, J. M. Oxygen reduction on nanostructured platinum surfaces in acidic media: Promoting effect of surface steps and ideal response of Pt(111). *Catalysis Today* **244,** 172–176 (2015).
19. Calle-Vallejo, F. *et al.* Why conclusions from platinum model surfaces do not necessarily lead to enhanced nanoparticle catalysts for the oxygen reduction reaction. *Chemical Science* **8,** 2283–2289 (2017).
20. Calle-Vallejo, F. *et al.* Finding optimal surface sites on heterogeneous catalysts by counting nearest neighbors. *Science* **350,** 185–189 (2015).
21. Van de Krol, R. in *Photoelectrochemical Hydrogen Production* (eds Van de Krol, R. & Grätzel, M.) 109 (Springer, Boston, MA, 2012).
22. Attard, G. A., Brew, A., Hunter, K., Sharman, J. & Wright, E. Specific adsorption of perchlorate anions on Pt{hkl} single crystal electrodes. *Phys. Chem. Chem. Phys.* **16,** 13689–13698 (2014).
23. Jung, S., McCrory, C., Ferrer, I. M., Peters, J. C. & Jaramillo, T. F. Benchmarking Nanoparticulate Metal Oxide Electrocatalysts for the Alkaline Water Oxidation Reaction. *J. Mater. Chem. A* (2015).
24. Villullas, H. & Teijelo, M. The hanging-meniscus rotating disk (HMRD) Part 1. Dependence of hydrodynamic behavior on experimental variables. *Journal of Electroanalytical Chemistry* **384,** 25–30 (1995).
25. Gomez, R., Orts, J. M., Alvarez-Ruiz, B. & Feliu, J. M. Effect of Temperature on Hydrogen Adsorption on Pt(111), Pt(110), and Pt(100) Electrodes in 0.1 M HClO4. *The Journal of Physical Chemistry B* **108,** 228–238 (2004).
26. Vidal-Iglesias, F. J., Arán-Ais, R. M., Solla-Gullón, J., Herrero, E. & Feliu, J. M. Electrochemical Characterization of Shape-Controlled Pt Nanoparticles in Different Supporting Electrolytes. *ACS Catalysis* **2,** 901–910 (2012).
27. Wakabayashi, N., Takeichi, M., Itagaki, M., Uchida, H. & Watanabe, M. Temperature-dependence of oxygen reduction activity at a platinum electrode in an acidic electrolyte solution investigated with a channel flow double electrode. *Journal of Electroanalytical Chemistry* **574,** 339–346 (2005).
28. Gómez-Marín, A. M., Rizo, R. & Feliu, J. M. Oxygen reduction reaction at Pt single crystals: a critical overview. *Catalysis Science & Technology* **4,** 1685 (2014).
29. Gómez-Marín, A., Feliu, J. & Edson, T. Reaction Mechanism for Oxygen Reduction on Platinum: Existence of a Fast Initial Chemical Step and a Soluble Species Different from H2O2. *ACS Catalysis* **8,** 7931–7943 (2018).
30. Attard, G. A. & Brew, A. Cyclic voltammetry and oxygen reduction activity of the Pt{110}-(1×1) surface. *Journal of Electroanalytical Chemistry* **747,** 123–129 (2015).
31. Armand, D. & Clavilier, J. Electrochemical behaviour of the (110) orientation of a platinum surface in acid medium: the role of anions. *Journal of Electroanalytical Chemistry and Interfacial Electrochemistry* **263,** 109–126 (1989).

32. Clavilier, J., El Achi, K. & Rodes, A. In situ probing of step and terrace sites on Pt(S)-[n(111) × (111)] electrodes. *Chemical Physics* **141,** 1–14 (1990).
33. Arblaster, J. W. Crystallographic Properties of Platinum. *Platinum Metals Review* **41,** 12–21 (1997).
34. Vanrenterghem, B. *et al.* Cutting the Gordian Knot of electrodeposition via controlled cathodic corrosion enabling the production of supported metal nanoparticles below 5 nm. *Applied Catalysis B: Environmental* **226,** 396–402 (2018).
35. Garcia, A. C. *et al.* Strong Impact of Platinum Surface Structure on Primary and Secondary Alcohol Oxidation during Electro-Oxidation of Glycerol. *ACS Catalysis* **6,** 4491–4500 (2016).
36. Vidal-Iglesias, F. J. *et al.* Shape-dependent electrocatalysis: Ammonia oxidation on platinum nanoparticles with preferential (100) surfaces. *Electrochemistry Communications* **6,** 1080–1084 (2004).